Morpho-sedimentary dynamics of a micro-tidal mixed sand and gravel beach, Playa Granada, southern Spain

Rafael J. Bergillos[a], Miguel Ortega-Sánchez[a], Gerd Masselink[b], Miguel A. Losada[a]

[a] *Andalusian Institute for Earth System Research, University of Granada, Avda. del Mediterráneo, s/n, 18006, Granada, Spain*
[b] *School of Marine Science and Engineering, Plymouth University, PL4 8AA, Drake Circus, Plymouth, UK*

Abstract

This paper addresses the changes in the morphology and sedimentology of a micro-tidal mixed sand and gravel beach (Playa Granada, southern Spain) forced by wave and water-level variations, and human intervention through nourishment. Monthly and storm event-driven beach surveys, consisting of topographical measurements and sediment sampling in two selected areas, were carried out over a one-year period. Three prevailing sediment fractions (sand, fine gravel and coarse gravel) and two end-member morphological states of the upper beach profile (convex with multiple berms and concave with a single storm berm) were identified. Between them, several transitional profiles were formed, characterized by developing berms that progressively overlapped, generating sediment variability both across the beach profile and with depth. The results indicate that the total run-up (including water-level) reached during an event represents a more accurate threshold for differentiating between erosional and depositional conditions than wave height. They also suggest that mixed sand and gravel beaches recover faster from storm erosion than sandy beaches. The long-term benefit of the artificial nourishment that took place at the end of the

*Corresponding author.
E-mail address: rbergillos@ugr.es (R.J. Bergillos)

survey period was very limited and this is attributed to the too fine sediment used for the nourishment and its placement too high on the beach. Clearly, nourishment interventions must take into account the natural sediment distribution and the profile shape to avoid rapid losses of the nourished sediment.
Keywords: Mixed sand and gravel beach, field measurements, beach profile, total run-up, artificial nourishment

1. Introduction

According to Jennings and Shulmeister (2002), two types of mixed sand/gravel beaches can be differentiated: (1) composite beaches, with a gravel high tide beach and a sandy low tide terrace; and (2) mixed sand and gravel beaches (MSGBs), with sand and gravel fractions mixed both cross-shore and at depth. Such beaches are globally less common than sandy beaches, but they are widespread in certain regions, such as previously (para-)glaciated areas (e.g., Ireland, UK, Canada) (Clemmensen et al., 2016) and coastlines with steep hinterlands (e.g., Mediterranean, New Zealand). The composite beach type, where the gravel and sand have been sorted by cross-shore processes, requires a tide range and is more common in meso- and macrotidal regions, whereas MSGBs are more common in micro-tidal coastal settings.

MSGBs are also found when replenishment schemes use a mixture of sand and gravel, often from the shelf, or when gravels are used to protect sandy beaches (López de San Román-Blanco, 2004). Although MSGBs have received increasing attention in recent years, numerous studies highlighted the discrepancy between the advances made for sandy beaches and the lack of similar progress for pure gravel and mixed sand/gravel beaches (Mason and Coates, 2001; Jennings and Shulmeister, 2002; Pontee et al., 2004; Buscombe and Masselink, 2006; López de San Román-Blanco et al., 2006; Horn and Walton, 2007). Foti and Blondeaux (1995) concluded that sediment transport processes and

morphological evolution on MSGBs are different and more complex than on sandy and pure gravel beaches.

The identification and characterization of the morphodynamic states of MSGB profiles are important for the correct management of these environments. Buscombe and Masselink (2006) introduced the concept of *morpho-sedimentary dynamics* as the mutual interactions of morphology, hydro-hydraulics and sediment properties, highlighting that it is the recommended conceptual framework within which to organise further research for gravel environments. This analysis is also relevant for the design of artificial nourishment to combat beach erosion (Li et al., 2006).

Previous studies on MSGBs focused on specific aspects: Horn and Walton (2007) described the sediment distribution before, during and after a nourishment program along a section of an MSGB and analysed the effects of sediment recharge with different sedimentary properties. Eikaas and Hemmingsen (2006) performed a field study that focused on some sediment properties of an MSGB, but did not address the morphological characteristics of the beach profile. Ivamy and Kench (2006) and Bramato et al. (2012) analysed the recovery of MSGBs after storms, but did not study the sedimentological aspects.

Hence, neither the morphological evolution of the beach as a result of wave and water-level forcing, nor its characteristic morpho-sedimentary states have been studied in depth for MSGBs. In addition, the contribution of wave run-up, astronomical tide and storm surge to the total run-up, and their roles in the beach response has not been explored in detail on micro-tidal coasts. These facts, along with the presence of MSGBs on many worldwide coasts, the frequent use of gravel to protect eroded sandy beaches (Van Wellen et al., 2000; Mason and Coates, 2001) and the expected sea-level rise in the coming years attest to the importance of this study.

The main objective of the article is to characterize the morphological and sedimentary dynamics of an MSGB, focusing on the contribution of wave run-up, storm surge and astronomical tide to natural beach response, as well as its behavior after artificial nourishment. To meet this objective, the evolution of wave and wind conditions and total run-up is analysed; the morphological and sedimentary characteristics of the beach are detailed; typical morpho-sedimentary states are identified; and the profile response before, during and after artificial replenishment is investigated. All morphological variability is related to the wave and water-level forcing.

2. Study site

Playa Granada is a 3-km-long micro-tidal MSGB located on the southern coast of the Iberian Peninsula that faces the Alborán Sea (Figure 1a). The beach corresponds to the central stretch of coast of the Guadalfeo deltaic system (Bergillos et al., 2015b) and is bounded to the west by the Guadalfeo River mouth and to the east by *Punta del Santo*, a former location of the river mouth (Figure 1b).

The Andalusian littoral of the Alborán Sea is characterized by the presence of high mountainous relief and short fluvial streams. The major contribution of sediments to the beach is provided by the Guadalfeo River. Its basin has an area of 1252 km^2, includes the highest peaks on the Iberian Peninsula (approximately 3400 m.a.s.l.), and is fed by one of the most high hydrological energy systems along the Spanish Mediterranean coast (Jabaloy-Sánchez et al., 2014). The topographic gradients lead to a wide range of sediment sizes in the Guadalfeo river sediment load (Millares et al., 2014).

Consequently, the particle size distribution in Playa Granada is particularly complex, with varying proportions of sand and gravel (Bergillos et al., 2015a).

This stretch of beach exhibits a broader range of sediment sizes (Losada et al., 2011) and has presented a higher coastline retreat in recent years (Félix et al., 2012) than both western and eastern stretches, known as Salobreña and Poniente Beach, respectively.

The climate at the study site exhibits a significant contrast between summer and winter. The region is subjected to the frequent passage of extratropical Atlantic and Mediterranean storms, which generate wind waves under limited fetch conditions (approximately 300 km) with average wind speeds of 18 to 22 m/s (Ortega-Sánchez et al., 2008). The prevailing wave directions are west-southwest and east-southeast (bimodal), whereas the 50%, 90% and 99% exceedance significant wave heights in deep water are 0.5 m, 1.2 m and 2.1 m, respectively.

3. Methodology

3.1. Data

3.1.1. Maritime data

One year of hourly hindcasted data, corresponding to WANA point number 2041080 (Figure 1a), was used for driving the wave-induced coastal morphological changes. The WANA networks wind fields are obtained through the High Resolution Limited Area Model (Cats and Wolters, 1996) and the wave fields are computed through the WAM model (Booij et al., 1999), on the basis of the wind field data (López et al., 2012). The following variables were extracted from these hindcasted data: deep-water significant wave height (H_0), spectral peak period (T_p), deep-water wave direction (θ_0), wind velocity (V_w) and wind direction (θ_w). Furthermore, the astronomical tide measured by a gauge located in the Motril Port was used to represent the tidal forcing. Both wave and tide data were provided by *Puertos del Estado*.

3.1.2. Field surveys

Field surveys were performed from October 2013 to September 2014 (hereafter referred to as the study period). To analyse the beach morphological evolution, two study areas within the study site were selected (Figure 2) to ensure the results were representative for entire beach section.

Monthly periodic field surveys were performed during the study period, consisting of topographic and sediment sizes measurements of the beach profile. In addition, several specific surveys were carried out before and after two significant storms (December 2013 and March 2014), and before, during and after the artificial replenishment of the beach performed in June 2014 (Table 1). Each survey was carried out under low tide conditions and the measurements were referenced to the mean low water spring level (MLWS) to avoid negative contributions of the astronomical tide to the total run-up. The two major storms that occurred during the study period were identified by means of the peaks over threshold (POT) method (Goda, 2010) considering $H_T = 3.1$ m ($H_{99.9\%}$) and storm durations lasting longer than 6 hours.

No. Survey	1	2	3	4	5	6	7	8	9
Date	25/10	22/11	20/12	27/12	10/1	21/1	27/2	10/3	17/3
Type of Survey	P	P	P	S	S	P	P	S	S
10	11	12	13	14	15	16	17	18	19
31/3	25/4	19/5	2/6	13/6	17/6	25/6	24/7	21/8	19/9
P	P	P	S	S	S	P	P	P	P

Table 1: Timeline of the periodic (P) and specific (S) surveys carried out during the study period.

The topography was recorded with a highly accurate DGPS (Javad Maxor) with no more than 2 cm of both horizontal and vertical instrument errors. Previously, the geodesic coordinates of the vertex *105582 Punta del Santo* were moved to the positions of the GPS-base in the study areas. Ten profiles were measured at each study area to obtain an alongshore-averaged profile to reduce the uncertainty associated with measurement errors and alongshore varibility (Figure 2). Sediment samples, both at the surface and at depth (0-30 cm), were

taken at three points of each profile (Figure 2) to capture the spatial variability in the sediment distribution. Sieve analyses of the sampled sediments in each study area were performed following the basic methods of Folk (1980) with grain size nomenclature according to Wentworth (1922).

3.1.3. Bathymetry

A high-resolution multibeam bathymetric survey was carried out in October 2013 (beginning of the study period) at the study site. The data were acquired using DGPS navigation referring to the WGS-84 ellipsoid. Accurate navigation and real-time pitch, roll, and heave were corrected. The multibeam data were also corrected for the water column velocity. These bathymetric data were used as the bottom boundary condition for the wave propagation model (Section 3.2).

3.2. Wave propagation model

The WAVE module of the Delft3D model (Lesser et al., 2004; Lesser, 2009), which is based on the spectral wave model SWAN (Holthuijsen et al., 1993), was applied (considering the WANA point data) to estimate inshore wave conditions. Simulated wave heights were obtained at points with depth of 8 m ($H_{8\mathrm{m}}$) to avoid the influence of wave breaking and these inshore wave conditions were related to the beach response. The model domain consisted of two different grids, shown in Figure 1c. The first grid is a coarse curvilinear 82x82 - cell grid covering the entire Playa Granada region, with cell sizes that decrease with depth from 88x60 to 48x35 m. The second grid is a nested grid with 82 and 144 cells in the alongshore and cross-shore directions, respectively, and cell sizes of about 25x14 m. This model was calibrated and successfully validated for the study site through comparison with field data by Bergillos et al. (2016).

3.3. Total run-up and sediment mobility formulations

3.3.1. Total run-up

The run-up measured on the beach by means of the DGPS (based on observations of run-up mark) was compared with estimates of the total run-up, obtained as the sum of astronomical tide, storm surge (wind set-up and inverse barometric effect) and wave run-up. The wind set-up was calculated as follows: $\Delta\eta_{\text{wind}} = \tau_{\text{wind}}/\rho g h_0 \cdot \Delta x$ (Bowden, 1983), where the depth of the wave base level is represented by $h_0 = L_0/4$, ΔX is the wave fetch from the centre of the low-pressure system to the coast (estimated through isobar maps) and the tangential wind stress is obtained from $\tau_{\text{wind}} = \rho_a U_*^2$, where ρ_a is the air density and U_* is the friction velocity. The barometric set-up was obtained from $\Delta\eta_{\text{bar}} = \Delta P_a/\rho g$ (Dean and Dalrymple, 2002), where ΔP_a represents the atmospheric pressure variation relative to the long-term average pressure at Motril Port. Finally, the wave run-up was calculated through the equation $\Delta\eta_{\text{wave}} = 0.36\, g^{0.5}\, H_{8,0}^{0.5} T_p \tan\beta$ (Nielsen and Hanslow, 1991), where $\tan\beta$ is the intertidal slope and $H_{8,0}$ is the modelled wave height at 8 m water depth ($H_{8\text{m}}$) de-shoaled to deep water using linear theory and assuming parallel bottom contours. This parameter allows accounting for the alongshore variability of the inshore wave height and is consistent with the run-up expression which requires deep-water wave height. This formulation for total run-up was successfully used and compared with high resolution images from a video camera by Bramato et al. (2012) deployed on another nearby mixed sand and gravel beach along the Mediterranean Spanish coast.

3.3.2. Sediment mobility

Sunamura and Takeda (1984) derived the following relationship to determine the accretion/erosion states of a beach:

$$\frac{H_{8,0}}{L_0} = C\ \left(\tan\bar{\beta}\right)^{-0.27}\left(\frac{D}{L_0}\right)^{0.67} \quad (1)$$

where $H_{8,0}/L_0$ is the deep-water wave steepness, L_0 is the deep-water wave length, $C = 18$ is an empirical constant, D is the grain size and $\tan\bar{\beta}$ is the average nearshore bottom slope to a water depth of 20 m. According to Sunamura and Takeda (1984), the beach erodes (accretes) when the left-hand side of the equation is greater (smaller) than the right-hand side. The difference (S_r) between both sides of the equation was calculated considering the prevailing sediment sizes measured in Playa Granada for each sea state and the results were related with the beach evolution. This equation, deduced for sandy beaches, was tested in the study site to analyse the role of the different fractions and to discuss its applicability to MSGBs.

4. Results

4.1. Wave and wind conditions

Figure 3 depicts the evolution of the wave and wind conditions during the study period. The deep-water significant wave height and spectral peak period were generally $H_0 < 1$ m (73% of the time) and $T_p < 6$ s (76% of the time), indicating that the beach predominantly experienced low energy waves. This agrees with the generally calm wave climate of this part of the Mediterranean Spanish coast (Ortega-Sánchez et al., 2014). The predominant deep-water wave directions were west-southwest and east-southeast, and the maximum T_p was 12 s and associated with easterly waves (Figure 3). This relatively high value for T_p (for the Mediterranean) has been exceeded 0.24% of the time since 1958. The prevailing wind velocity was less than 10 m/s with incoming directions from the east-southeast and west-southwest. The latter was more frequent and

was generally associated with higher velocities. The wind direction was closely related to the wave direction.

Applying the POT method, two storms occurred that had maximum H_0 of 4.6 m and 4 m, and maximum $H_{8\mathrm{m}}$ of 3.6 m and 3.2 m in study area 1 and $H_{8\mathrm{m}}$ of 3.8 m and 3.3 m in study area 2. Both storms were associated with westerly waves ($\theta_0 \sim 240°$), with maximum T_p of 9.6 s and 8.8 s (Figure 3). The maximum V_w during storms 1 and 2 was 19.4 m/s and the θ_w was ~ 260 °. Both two storm events had a very high energy content compared to other storms that occurred in the Alborán Sea. Specifically, storm 1 was the third most severe since 1958 to the end of the study period, based on the WANA 2041080 data.

4.2. Water-level conditions: contributions to the total run-up

Figure 4a shows the time series of the maximum daily total run-up (referenced to the MLWS) in study area 1 estimated using the formulations described in Section 3.3.1; the relative contributions of the different contributors (astronomical tide, storm surge and wave run-up) to the total run-up are depicted in Figure 4b. The results for study area 2 were very similar (differences less than 5%), and are not shown. Comparison of the estimated maximum run-up values with those observed during 21 field measurements (19 during field surveys and 2 during storms) yielded high correlation (differences less than 9%), inspiring confidence in the estimated total run-up time series.

The measured tidal ranges during storms 1 and 2 were 0.2 m and 0.44 m, respectively, and were considerably less than the maximum tide range of 0.6 m (Figure 4a). This reinforces that the contribution of the astronomical tide to the total run-up under high-energy conditions is relatively minor, representing less than 21% for both storms (Figure 4b). In addition to wave run-up, storm surge is also a significant contributor to the total run-up, contributing more

than 30% during both storms (Figure 4b). The contribution of wave run-up reached values of almost 55% and 70% after storms 1 and 2 (recovery phases), i.e., between surveys 4-5 and 8-9, respectively (Figure 4b).

Waves are frequently considered as the main driver of changes in the profile of micro-tidal beaches. However, Figure 4b indicates that storm surge resulting from low atmospheric pressure and wind stress can also be important contributors to the total elevation under storm conditions and, consequently, to the erosion of the beach. If wind velocities are high enough ($V_w \sim 15$ m/s) and pressure gradients are negative, the resulting large storm surge enables waves to reach the upper parts of the beach profile (backshore), as shown in Figure 4a.

4.3. Morphological response of the upper profile

A total of 190 upper profiles (beach profile above the MLWS level) were measured during the study period in each study area: 130 before the artificial replenishment (natural profile) and 60 both during the nourishment and afterwards (replenished). Table 2 shows that the beach width (cross-shore distance between the MLWS level and the nearest building) and unit volume (calculated by the trapezoidal rule) of the beach typically increases under low energy conditions (LE) and decreases after storms (S). The slope of the natural profile, defined by the ratio between the height of beach crest and the beach width, was $0.05 - 0.069$ and $0.056 - 0.073$ in study areas 1 and 2, respectively.

		Study area 1	Study area 2
Natural profiles	Slope	0.05 (LE) − 0.069 (S)	0.056 (LE) − 0.073 (S)
	Beach width (m)	24.74 (S) − 35 (LE)	39.5 (S) − 50 (LE)
	Unit volume (m^2)	27 (S) − 41.40 (LE)	51.19 (S) − 73.56 (LE)
Replenished profiles	Slope	$0.057 - 0.059$	$0.05 - 0.053$
	Beach width (m)	$33.22 - 34.72$	$47 - 50$
	Unit volume (m^2)	$39.17 - 45.38$	$77.88 - 87.69$

Table 2: Morphological characteristics of the natural and replenished profiles in the study areas. LE: low energy conditions, S: storms.

Figure 5 depicts both the maximum wave height and total run-up (including

astronomical tide, storm surge and wave run-up) before each survey along with the sediment volume of the upper profile in both study areas (in m^3 per unit m beach length per day, or m^2/day). It is observed that beach erosion/accretion not only depends on wave height, but on the sum of the three components that contribute to the total run-up. Actually, a relationship between the maximum total run-up between surveys and the beach response is clearly observed, specially after the two storms (surveys 4 and 8).

The differences between the bed elevation in each survey and the average profile in study area 1 are also shown in Figure 5 (lower panel). During storms 1 and 2, the erosion rates in study area 1 were 2.06 and 1.09 m^2/day, respectively; whereas they were 3.2 and 1.76 m^2/day in study area 2. If a beach overwashes, erosion tends to be less, because the wave energy is dissipated across the backshore and sediment is retained within the beach in the form of overwash deposit (Matias et al., 2013, 2015). This occurred in both study areas during storms, as the entire beach was overwashed. On the other hand, the recovery rates after the storm 1 and 2 were at least 0.79 and 0.51 m^2/day in study area 1, and 1.76 and 0.94 in study area 2, respectively. It is important to highlight that these values are average rates between surveys, so the maximum erosion/accretion rates were most likely higher.

The profiles of both study areas were flattened due to the artificial nourishment carried out in June 2014. It consisted of an input of 8.4 m^3/m and 14 m^3/m in study areas 1 and 2 over beach lengths equal to 500 and 300 m, respectively. The slope of the replenished profiles was slightly milder than those of the pre-nourished beach, but higher than the slope under low energy conditions (Table 2). The sediment volume of the replenished profiles was greater than that of most natural profiles, although the width was similar to those of the natural profiles under low energy conditions (Table 2).

Figure 6 shows the evolution of the upper profile in study area 1 since the artificial replenishment to the end of the study period. Only one month after the artificial replenishment, and under prevailing low energy conditions and total run-up lower than 1.4 m until survey 17 (Figures 3 and 4a), the unit volume loss was about 2.6 m^2 in study area 1 and 3.3 m^2 in study area 2. Berms started to appear due to the total run-up attained during this period (Figures 5 and 6).

Between surveys 17 and 18, the profile shape also changed significantly in both study areas, but the variation was less between surveys 18 and 19 (Figures 5 and 6), most likely due to the smaller magnitude of the forcing agents and the total run-up (Figures 3 and 4a). The attenuation of the system response after the discharge of sediments could be another cause of this lower variation. However, not only wave processes, but also the gusts of wind after the nourishment project could contribute to the rapid loss of fine sediments, considering that wind velocities reached maximum values of 14.5 m/s and 13.5 m/s before surveys 17 and 18, respectively (Figure 3).

Altogether, the beach width in study areas 1 and 2 decreased by approximately 4% and 6% in the months after the nourishment, respectively, whereas the unit volume loss was 6.2 m^3/m in study area 1 and 9.8 m^3/m in study area 2. Furthermore, despite the artificial replenishment, the unit volumes measured in study areas 1 and 2 in September 2014 (39.16 m^2 and 77.8 m^2) were similar to those measured in October 2013 (38.74 m^2 and 73.03 m^2), as shown in Figure 5. Thus, the long-term benefit of the nourishment was very limited.

4.4. Beach sediments

The average grain size distribution (based on all sediment samples) before the artificial replenishment (Figure 7a) shows that three sediment fractions are predominant in Playa Granada: sand ($D_1 = 0.25 - 0.5$ mm, Figure 7c), fine gravel ($D_2 = 2 - 8$ mm, Figure 7d) and coarse gravel ($D_3 = 8 - 32$ mm, Figure

7e). The foreshore (from the MLWS to the maximum total run-up reached under low energy conditions) showed greater sediment size variability than the backshore in both study areas, as shown in Section 4.5. In addition to this cross-shore variability, different levels of gradation at depth were also found. The sand-gravel ratio limits were $30-70\%$ and $36-64\%$ in study area 1, and $33-67\%$ and $23-77\%$ in study area 2.

The nourished material (Figure 8a), shown in Figure 7b, was significantly finer than the natural sediment ($D_{50} = 1.92$ mm *vs* $D_{50} = 4.35$ mm). Coarse sand ($1-2$ mm) and fine gravel ($2-8$ mm) dominated (Figure 7f), with a sand-gravel ratio of about $52.5\% - 47.5\%$. Thus, the sand fraction of the nourished sediment was higher than that of the native sediment. After the nourishment, the sand-gravel ratio progressively reduced from its initial value ($52.5\%-47.5\%$) to about $46.15\% - 53.35\%$ and $41.65\% - 58.35\%$ in study areas 1 and 2, respectively. Therefore, the reduction in the percentage of sand was higher in study area 2, where the unit volume loss was also higher (Table 2).

Figure 9 shows the results of applying the formulation of Sunamura and Takeda (1984) during the study period. Considering the three prevailing sediment fractions in the study site (D_1, D_2 and D_3), the erosion ($S_r > 0$) and accretion ($S_r < 0$) states alternated for the sand fraction (Figure 9a, upper panel), while for the two gravel fractions only deposition states occurred (Figure 9a, middle and lower panels). These results are similar to those obtained by Bramato et al. (2012) through application of this formulation and observations based on high-resolution images for an MSGB near the study site: sand was transported offshore during storms and beach recovery was limited to low-energy sea states, whereas only onshore migration took place for the gravels.

4.5. Morpho-sedimentary beach states

4.5.1. Low energy state

Under prevailing low energy conditions, the upper profile in study area 1 has two berms (B1 and B2, Figure 10a) composed of a surface layer of coarse gravels ($D_1 = 8 - 32$ mm), a subsurface layer of fine gravels ($D_2 = 2 - 8$ mm), and a layer of sand ($D_3 = 0.25 - 0.5$ mm) at the base of the deposit (Figure 10a). This pattern is repeated at depth, probably reflecting previous berm deposits. The average percentage of sand-gravel along the sampled sediment layer is $35.8\% - 64.2\%$. The backshore (cross-shore distance < 15 m, Figure 10a) consists mainly of sand (Table 3), whereas the composition of the sediment in the active swash zone is highly variable (sand-fine gravel) in time and space (Figure 10a), with average proportions of 31.7% sand and 68.3% gravel. The upper profile in study area 2 is similar to that of the study area 1, but the beach is wider (~ 50 m). The average sand-gravel ratio sampled across the entire upper profile for study area 1 is larger than for study area 2 (Table 3).

4.5.2. Storm state

The two storms that occurred over the survey period (1 and 2, Figure 3) induced marked changes to the beach profile. The low energy state berms were eroded and the upper beach profiles assumed a more concave shape (Figure 10b). The storms also caused a decrease in the beach width of about 5 m and 10 m in study areas 1 and 2, respectively. A storm berm developed on the upper part of the profile and a bar feature was generated in the lower part of the beach with a surface layer of sand over a gravel-dominated substrate (Figures 8b and 10b). In both study profiles, higher slopes were generally attained during storm conditions and the percentage of gravel increased by between 6 and 10 percent from the low energy state to the storm state (Table 3).

Considering the total number of samples taken after the two storms (18) and

during the low energy states of the profile (27) in study area 1 and applying the *Student's t-test*, the result also confirm that the percentage of gravel is higher after storms (null hypothesis), with a significance level equal to 0.01. The same conclusion is drawn after applying the test in study area 2. These results are consistent with those obtained in Section 4.4: the finer material is selective transported offshore during storms, whereas under calm conditions the sand returns, covering most of the lag gravel (Figure 10). This is a mechanism that differentiate MSGBs from sandy and pure gravel beaches (Mason and Coates, 2001; Bramato et al., 2012).

		Low energy state	Storm state
Study area 1	Backshore	81.8% − 18.2%	34.8% − 65.2%
	Foreshore	31.7% − 68.3%	24.8% − 75.2%
	Entire beach	35.8% − 64.2%	29.2% − 70.8%
Study area 2	Backshore	80.8% − 19.2%	31.1% − 68.9%
	Foreshore	30% − 70%	19.7% − 80.3%
	Entire beach	33.1% − 66.9%	23.7% − 76.3%

Table 3: Sand-gravel percentages for the low energy and storm states on the backshore, foreshore and entire beach.

4.5.3. Transitional states

After the passing of storms, berms developed and progressively overlapped under the influence of low energy waves, contributing to the sediment variability both cross-shore and at depth (Figure 11). The generation of berms represents a recovery trajectory, which is closely related to the total run-up (Figures 4, 5 and 11), but this development of the berms can be interrupted at any one time by another storm. Figure 5 shows that the erosion/deposition rates were higher in the foreshore, where the measured sediment variability was also higher (Table 3). This is consistent with the conceptual model presented in Figure 11, which suggests that the number of berms depends on the state of the profile and varies during the recovery process.

Figure 12a depicts the contribution of the wave run-up (vertical axis) and the sum of astronomical tide and storm surge (horizontal axis) to the unit volume

variation (circles). Before the replenishment, it is observed that when the total run-up elevation was higher than the height of the upper berm ($\sim$ 1.52 m, Figure 10a), the upper profile lost volume, whereas lower elevations increased the volume of the beach (Figure 12a). Hence, beach erosion took place not only during both storms, when overwashing of the entire beach occurred; but also before surveys 2, 6 and 11, when the upper berm was overwashed.

Although the total run-up was similar in both study areas and the erosion/accretion behaviour of the upper profile was equal (Figure 5, middle panel), the threshold elevation in study area 2 was $\sim$ 1.58 m (Figure 12b), coinciding with the height of the upper berm at this profile. These results indicate that the overwash process plays a key role in the beach dynamics, which is in agreement with previous works, such as Matias et al. (2014). Hence, other variables apart from wave height, such as pressure gradient and wind velocity, are essential in the evolution of the profile on micro-tidal beaches and the total run-up is demonstrated to be a more accurate threshold than wave height to differentiate between erosional and depositional conditions.

5. Discussion

Although MSGBs have received increasing attention in recent years, the number of field observations on these coastal settings is still limited. This study presents the first detailed field investigation of the morpho-sedimentary dynamics of a MSGB under varying wave and water-level conditions.

The low energy states found on the studied beach are similar to those observed on a sandy beach (Avoca, New South Wales, Australia) and a pure gravel beach (Slapton Sands, Devon, UK) by Weir et al. (2006) and Austin and Masselink (2006), respectively. They proposed that berm location(s) is (are) linked to both tide level and wave run-up, and their destruction and construction de-

pends on wave height. The location of the upper berm and the process of berm formation in Playa Granada are also related to the maximum water-level elevation on the beach under low energy conditions and the wave action (Figures 4a, 5 and 10a). The generation and subsequent overlapping of berms is responsible for the different levels of grain size gradation at depth and cross-shore (Figure 11), that is, the evolutionary pathway is responsible for the beach stratification, being the morphological evolution partly stored in the stratigraphy. However, the results indicate that not only wave height, but also storm surge is important for the destruction of berms on micro-tidal beaches.

The storm berm and the bar feature observed following the storms resemble the eroded state on other MSGB of the Mediterranean Spanish coast (Carchuna) described by Bramato et al. (2012). They found that the profile after high energetic events promotes wave breaking over a newly formed storm bar, resulting in less capacity to transport sediments and protecting the beach from further erosion. The steeper shape of the upper profile after storm is also similar to the reflective morphodynamic state detailed by Poate et al. (2013) on the gravel beach of Loe Bar (Cornwall, UK), who also measured a depositional feature in the foreshore similar to that of Playa Granada (Figures 8 and 10b). This bar feature could be associated with the landward migration and growth of the beach step during storms coincident with the removal and offshore transport of the sand fractions from the swash zone, according to the morphological response found by Masselink et al. (2010) on Slapton Sands.

The evolution of both study areas was similar during the study period (Figures 5 and 12), indicating that they are representative of the beach behaviour of that section of the coastline. Comparing the measured slopes of the natural profiles (Table 2) with other published data, these slopes are generally steeper than on micro-tidal sandy beaches (Jackson et al., 2005), but gentler than the

slope on macrotidal gravel beaches analyzed by Austin and Masselink (2006) and Poate et al. (2013), and the slope on the MSGB described in Horn and Walton (2007). The observed slope is slightly steeper than that measured on another micro-tidal MSGB along the southern Spanish coast (Bramato et al., 2012).

The results obtained in Section 4.4 for the sand (alternation of erosion and accretion states) are more related with the beach behaviour than those for gravel fractions (only accretion); however, erosion states prevail for the sand fraction (Figure 9) whereas beach accretion was more frequent before the nourishment (Figure 12). They suggest that the overall behaviour of MSGBs cannot simply be determined by a single sediment size. Actually, the recovery periods (rates) in the study site after the third most severe storm since 1958, less than two weeks, were significant lower (higher) than those detailed by Lee et al. (1998), Thom and Hall (1991) and Scott et al. (2015), who measured average recovery rates of about 0.09 m^2/day, 0.11 m^2/day and 0.26 m^2/day on the sandy beaches of Duck (US), Moruya (Australia) and Perranporth (UK), respectively. This supports the conclusions of Mason et al. (1997) and Ivamy and Kench (2006): MSGBs may experience more active sediment transport than sandy beaches.

Replenished profiles were eroded even under no storm conditions (Figures 3, 5 and 6) and the unit volumes of the upper profiles 3 months after the nourishment (September 2014) were similar to those measured at the beginning of the study period (October 2013), when no artificial replenishment took place. This may be partly due to the lack of response from the nourished material to waves in the same manner as natural beaches (Horn and Walton, 2007). Dean and Dalrymple (2002) suggested that the fill material should match the native sediment to minimize changes in the beach response. This did not happen in Playa Granada, where neither the sediment sizes nor the morphology of the natural

and replenishment profiles were similar (Figures 7 and 6). The variations in the sand-gravel ratio after the artificial nourishment agree with the formulation of Sunamura and Takeda (1984), which establishes that the eroded sediment appeared to be selectively transported offshore from the upper profile. However, wind action could also have contributed to the removal of the finer nourished sediment, as has been widely demonstrated in previous works (e.g, Van der Wal (1998, 2000a,b); Jackson and Nordstrom (2011)).

6. Conclusions

1. The generation and subsequent overlapping of berms is responsible for the sediment variability cross-shore and at depth on MSGBs. The cross-shore locations of these berms are related to the total run-up, as berms are modified by swash action. Thus, waves play a main role in the beach recovery, and the recovery appears to be occurring at a faster rate than on sandy beaches.
2. The formation of a storm berm, the more concave shape of the upper profile and the increase in the percentage of gravels after storms all indicate reflective behaviour of MSGBs during high-energy conditions, and is dominated by the gravel fractions due to the selective removal of the finer material.
3. Total run-up elevations that exceed the height of the upper berm generate erosion, whereas lower elevations increase the unit volume of the upper profile representative of beach accretion. Hence, the total run-up represents a more accurate threshold dictating beach response than wave height.
4. The upper profile was flattened following an artificial input of sediment over June 2014 with different grain size distribution and lower D_{50} than

the natural sediment. Three months after the nourishment, and in the absence of significant storms, the upper profile lost between 6 and 10 m^2, probably induced by both wave processes and wind action. The beach volumes in September 2014 were similar to those measured in October 2013, showing the intervention was not effective.

Acknowledgments

This research was supported by the project CTM2012-32439 (Secretara de Estado de I+D+i, Spain) and the research group TEP-209 (Junta de Andaluca). The work of the first author was funded by the Ministry of Economy and Competitiveness (Spain) through Research Contract BES-2013-062617 and Mobility Grant EEBB-I-15-10002. We thank Servicio Provincial de Costas (Granada, Spain) for providing information about the artificial replenishment of the beach and Miguel A. Reyes-Merlo for his support with the field surveys. Finally, we would like to acknowledge the Editor and two anonymous reviewers for their improvements to this paper.

References

Austin, M.J., Masselink, G., 2006. Observations of morphological change and sediment transport on a steep gravel beach. Marine Geology 229, 59–77.

Bergillos, R.J., Delgado-Rodríguez, C., López-Ruiz, A., Millares, A., Ortega-Sánchez, M., Losada, M.A., 2015a. Recent human-induced coastal changes in the Guadalfeo river deltaic system (southern Spain), in: Proceedings of the 36th IAHR-International Association for Hydro-Environment Engineering and Research World Congress: http://89.31.100.18/ iahrpapers/87178.pdf.

503 Bergillos, R.J., López-Ruiz, A., Ortega-Sánchez, M., Masselink, G., Losada,
504 M.A., 2016. Implications of delta retreat on wave propagation and longshore
505 sediment transport - Guadalfeo case study (southern Spain). Marine Geology
506 , Under review.

507 Bergillos, R.J., Ortega-Snchez, M., Masselink, G., Losada, M.A., 2015b. Ur-
508 ban planning analysis of mediterranean deltas - Guadalfeo case study, in:
509 12th International Conference on the Mediterranean Coastal Environment,
510 MEDCOAST 2015, pp. 143–154.

511 Booij, N., Ris, R., Holthuijsen, L.H., 1999. A third-generation wave model for
512 coastal regions: 1. Model description and validation. Journal of Geophysical
513 Research: Oceans (1978–2012) 104, 7649–7666.

514 Bowden, K.F., 1983. Physical oceanography of coastal waters. Ellis Horwood
515 Ltd., Chichester England.

516 Bramato, S., Ortega-Sánchez, M., Mans, C., Losada, M.A., 2012. Natural re-
517 covery of a mixed sand and gravel beach after a sequence of a short duration
518 storm and moderate sea states. Journal of Coastal Research 28, 89–101.

519 Buscombe, D., Masselink, G., 2006. Concepts in gravel beach dynamics. Earth-
520 Science Reviews 79, 33–52.

521 Cats, G., Wolters, L., 1996. The Hirlam project [meteorology]. Computational
522 Science & Engineering, IEEE 3, 4–7.

523 Clemmensen, L.B., Glad, A.C., Kroon, A., 2016. Storm flood impacts along
524 the shores of micro-tidal inland seas: A morphological and sedimentological
525 study of the Vesterlyng beach, the Belt Sea, Denmark. Geomorphology 253,
526 251–261.

Dean, R., Dalrymple, R., 2002. Coastal processes with engineering applications Cambridge University Press. New York .

Eikaas, H.S., Hemmingsen, M.A., 2006. A GIS approach to model sediment reduction susceptibility of mixed sand and gravel beaches. Environmental management 37, 816–825.

Félix, A., Baquerizo, A., Santiago, J., Losada, M., 2012. Coastal zone management with stochastic multi-criteria analysis. Journal of environmental management 112, 252–266.

Folk, R.L., 1980. Petrology of sedimentary rocks. Hemphill Publishing Company.

Foti, E., Blondeaux, P., 1995. Sea ripple formation: the heterogeneous sediment case. Coastal Engineering 25, 237–253.

Goda, Y., 2010. Random seas and design of maritime structures. World Scientific.

Holthuijsen, L., Booij, N., Ris, R., 1993. A spectral wave model for the coastal zone, in: Ocean Wave Measurement and Analysis (1993), ASCE. pp. 630–641.

Horn, D.P., Walton, S.M., 2007. Spatial and temporal variations of sediment size on a mixed sand and gravel beach. Sedimentary Geology 202, 509–528.

Ivamy, M.C., Kench, P.S., 2006. Hydrodynamics and morphological adjustment of a mixed sand and gravel beach, Torere, Bay of Plenty, New Zealand. Marine Geology 228, 137–152.

Jabaloy-Sánchez, A., Lobo, F.J., Azor, A., Martín-Rosales, W., Pérez-Peña, J.V., Bárcenas, P., Macías, J., Fernández-Salas, L.M., Vázquez-Vílchez, M., 2014. Six thousand years of coastline evolution in the Guadalfeo deltaic system (southern Iberian Peninsula). Geomorphology 206, 374–391.

552 Jackson, D., Cooper, J., Del Rio, L., 2005. Geological control of beach morpho-
553 dynamic state. Marine Geology 216, 297–314.

554 Jackson, N.L., Nordstrom, K.F., 2011. Aeolian sediment transport and land-
555 forms in managed coastal systems: a review. Aeolian research 3, 181–196.

556 Jennings, R., Shulmeister, J., 2002. A field based classification scheme for gravel
557 beaches. Marine Geology 186, 211–228.

558 Lee, G.h., Nicholls, R.J., Birkemeier, W.A., 1998. Storm-driven variability of the
559 beach-nearshore profile at Duck, North Carolina, USA, 1981–1991. Marine
560 geology 148, 163–177.

561 Lesser, G., Roelvink, J., Van Kester, J., Stelling, G., 2004. Development and
562 validation of a three-dimensional morphological model. Coastal engineering
563 51, 883–915.

564 Lesser, G.R., 2009. An approach to medium-term coastal morphological mod-
565 eling. Ph.D. thesis. Department of Civil Engineering, Delft University of
566 Technology, Delft, The Netherlands.

567 Li, F., Dyt, C., Griffiths, C., 2006. Multigrain sedimentation/erosion model
568 based on cross-shore equilibrium sediment distribution: application to nour-
569 ishment design. Estuarine, Coastal and Shelf Science 67, 664–672.

570 López, M., López, I., Iglesias, G., 2012. Hindcasting Long Waves in a Port: An
571 ANN Approach. Coastal Engineering Journal , 1550019.

572 López de San Román-Blanco, B., 2004. Dynamics of gravel and mixed sand and
573 gravel beaches. Ph.D. thesis. Imperial College, London.

574 López de San Román-Blanco, B., Coates, T.T., Holmes, P., Chadwick, A.J.,
575 Bradbury, A., Baldock, T.E., Pedrozo-Acuña, A., Lawrence, J., Grüne, J.,

2006. Large scale experiments on gravel and mixed beaches: Experimental procedure, data documentation and initial results. Coastal engineering 53, 349–362.

Losada, M.A., Baquerizo, A., Ortega-Sánchez, M., Ávila, A., 2011. Coastal evolution, sea level, and assessment of intrinsic uncertainty. Journal of Coastal Research , 218–228.

Mason, T., Coates, T., 2001. Sediment transport processes on mixed beaches: a review for shoreline management. Journal of Coastal Research , 645–657.

Mason, T., Voulgaris, G., Simmonds, D.J., Collins, M.B., 1997. Hydrodynamics and sediment transport on composite (Mixed Sand/Shingle) and sand beaches: a comparison, in: Coastal Dynamics, ASCE. pp. 48–57.

Masselink, G., Russell, P., Blenkinsopp, C., Turner, I., 2010. Swash zone sediment transport, step dynamics and morphological response on a gravel beach. Marine Geology 274, 50–68.

Matias, A., Blenkinsopp, C.E., Masselink, G., 2014. Detailed investigation of overwash on a gravel barrier. Marine Geology 350, 27–38.

Matias, A., Masselink, G., Castelle, B., Blenkinsopp, C.E., Kroon, A., 2015. Measurements of morphodynamic and hydrodynamic overwash processes in a large-scale wave flume. Coastal Engineering .

Matias, A., Masselink, G., Kroon, A., Blenkinsopp, C.E., Turner, I.L., 2013. Overwash experiment on a sandy barrier. Journal of Coastal Research 1, 778.

Millares, A., Polo, M., Moñino, A., Herrero, J., Losada, M., 2014. Bedload dynamics and associated snowmelt influence in mountainous and semiarid alluvial rivers. Geomorphology 206, 330–342.

Nielsen, P., Hanslow, D.J., 1991. Wave runup distributions on natural beaches. Journal of Coastal Research , 1139–1152.

Ortega-Sánchez, M., Bramato, S., Quevedo, E., Mans, C., Losada, M.A., 2008. Atmospheric-hydrodynamic coupling in the nearshore. Geophysical Research Letters 35.

Ortega-Sánchez, M., Lobo, F., López-Ruiz, A., Losada, M., Fernández-Salas, L., 2014. The influence of shelf-indenting canyons and infralittoral prograding wedges on coastal morphology: The Carchuna system in Southern Spain. Marine Geology 347, 107–122.

Poate, T., Masselink, G., Davidson, M., McCall, R., Russell, P., Turner, I., 2013. High frequency in-situ field measurements of morphological response on a fine gravel beach during energetic wave conditions. Marine Geology 342, 1–13.

Pontee, N.I., Pye, K., Blott, S.J., 2004. Morphodynamic behaviour and sedimentary variation of mixed sand and gravel beaches, Suffolk, UK. Journal of Coastal Research , 256–276.

Scott, T., Masselink, G., O'Hare, T.A., Davidson, M., Russell, P., 2015. Multi-annual sand and gravel beach response to storms in the southwest of England, in: Proceedings of the 8th Coastal Sediments.

Sunamura, T., Takeda, I., 1984. Landward migration of inner bars. Developments in Sedimentology 39, 63–78.

Thom, B., Hall, W., 1991. Behaviour of beach profiles during accretion and erosion dominated periods. Earth Surface Processes and Landforms 16, 113–127.

624 Van Wellen, E., Chadwick, A., Mason, T., 2000. A review and assessment of
625 longshore sediment transport equations for coarse-grained beaches. Coastal
626 Engineering 40, 243–275.

627 Van der Wal, D., 1998. Effects of fetch and surface texture on aeolian sand
628 transport on two nourished beaches. Journal of Arid Environments 39, 533–
629 547.

630 Van der Wal, D., 2000a. Grain-size-selective aeolian sand transport on a nour-
631 ished beach. Journal of Coastal Research , 896–908.

632 Van der Wal, D., 2000b. Modelling aeolian sand transport and morphological
633 development in two beach nourishment areas. Earth Surface Processes and
634 Landforms 25, 77–92.

635 Weir, F.M., Hughes, M.G., Baldock, T.E., 2006. Beach face and berm morpho-
636 dynamics fronting a coastal lagoon. Geomorphology 82, 331–346.

637 Wentworth, C.K., 1922. A scale of grade and class terms for clastic sediments.
638 The Journal of Geology , 377–392.

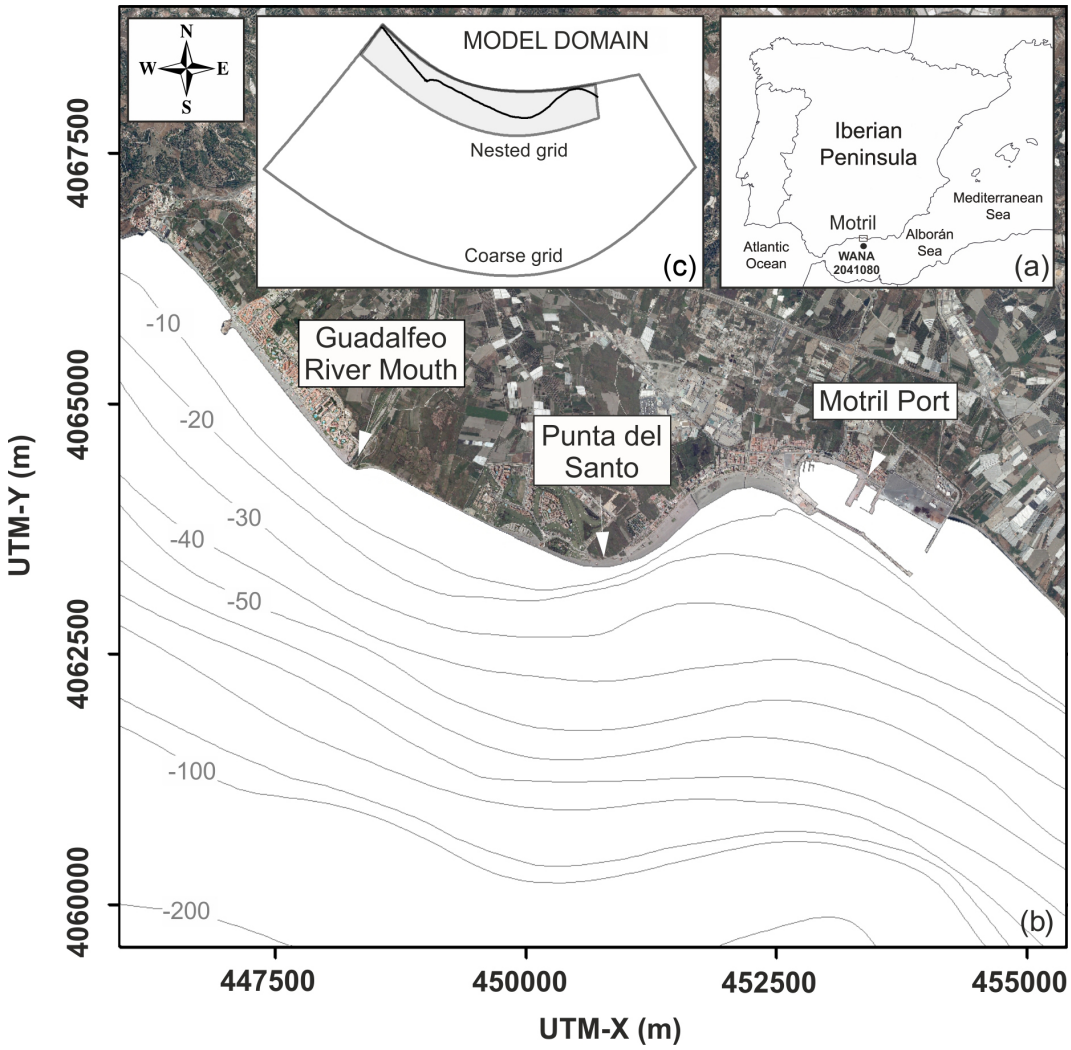

Figure 1: (a) Location of the study site (Playa Granada, southern Spain) and the WANA point 2041080. (b) Delimitation of the study site (Guadalfeo River mouth - Motril Port) and bathymetric contours (in meters below the MLWS level). (c) Boundaries of the computational grids used in the numerical model.

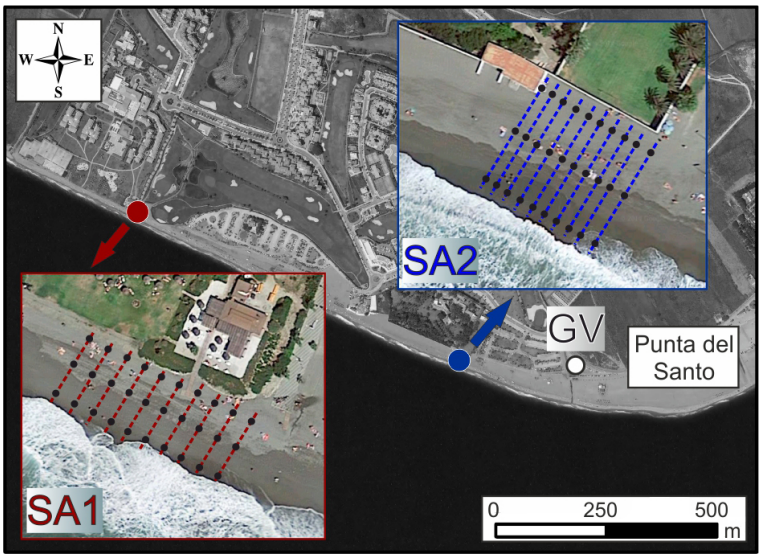

Figure 2: Selected study areas and geodesic vertex *Punta del Santo*. Ten profiles were measured in both study areas (dashed lines) and samples were taken both at the surface and at depth in each profile (dots).

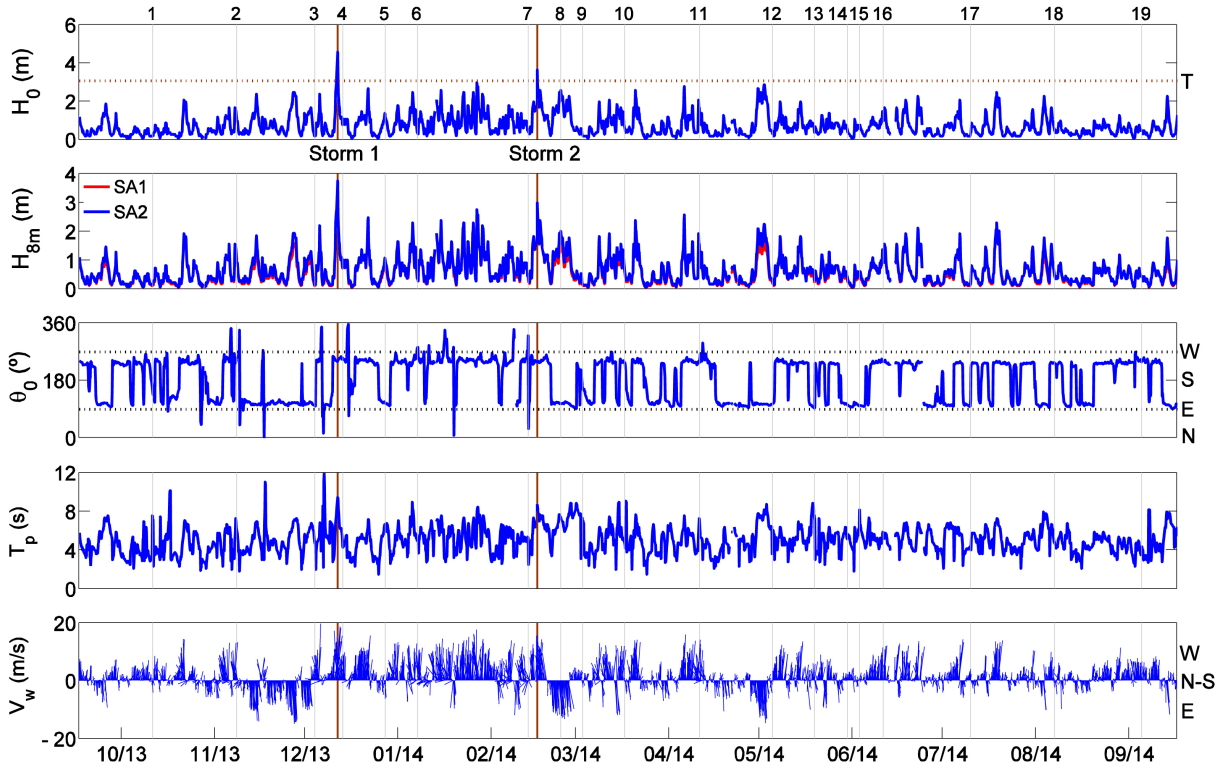

Figure 3: From top to bottom: evolution of the deep-water wave height, wave height at depths of 8 m (red: study area 1, blue: study area 2), deep-water wave direction, spectral peak period, and wind velocity and direction. The vertical lines (grey) indicate the date of the field surveys and storms are marked in brown.

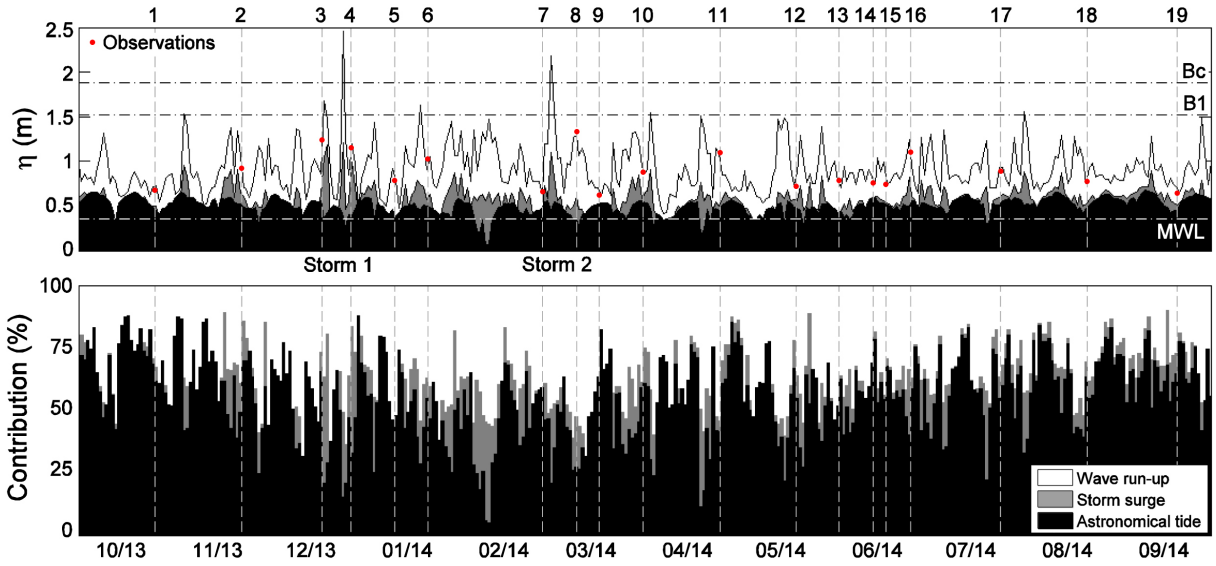

Figure 4: (a) Evolution of the astronomical tide, storm surge and wave run-up and (b) contribution of each in the study area 1 during the study period. $\eta = 0$ indicates the MLWS level and the vertical lines (grey) indicate the date of the field surveys. The observations of total run-up (red circles), height of the mean water-level (MWL), the beach crest (Bc) and the upper berm (B1) are indicated.

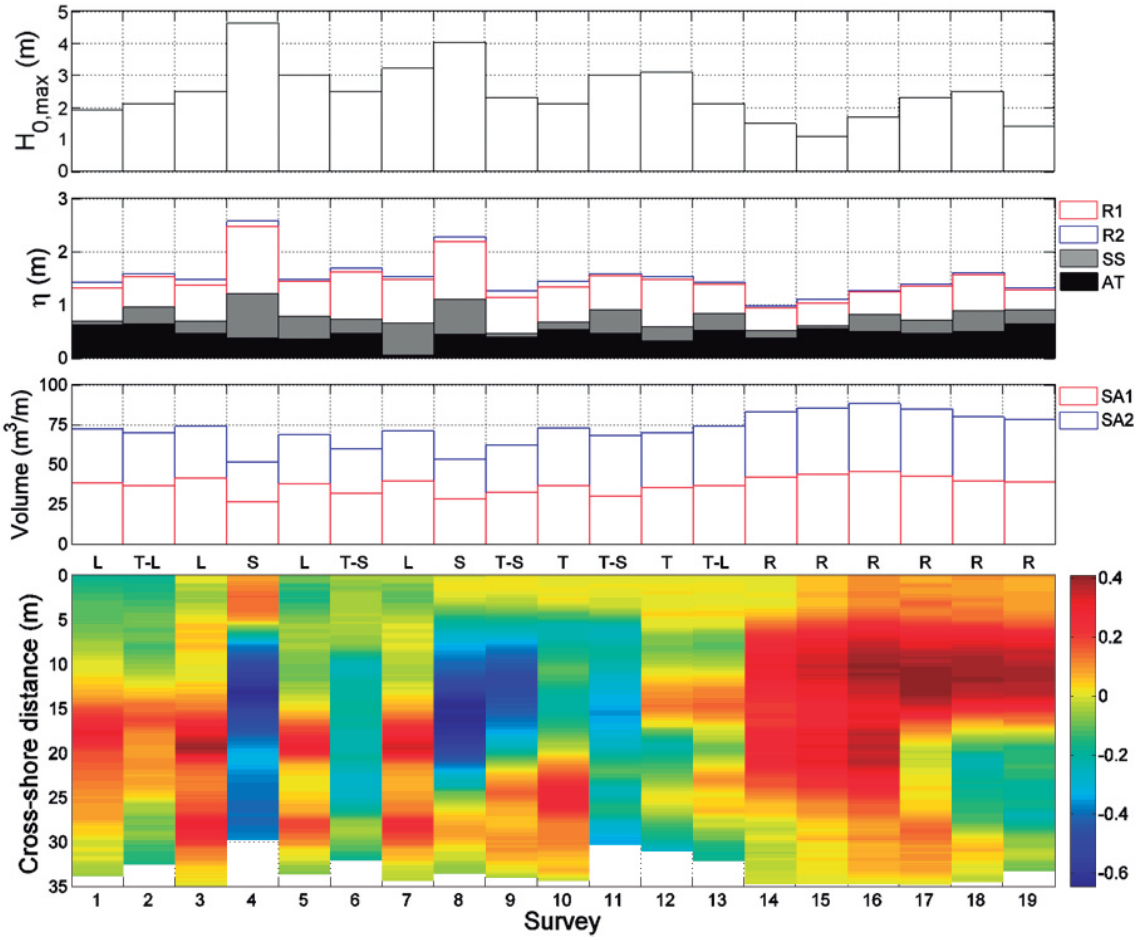

Figure 5: From top to bottom: maximum deep-water wave height before each survey; astronomical tide (black), storm surge (grey) and wave run-up (red: study area 1, blue: study area 2) contributions to the maximum total run-up before each survey; unit volume of the upper profile (red: study area 1, blue: study area 2); and differences between the profile in each survey and the average profile in study area 1. States of the profile, according to Figure 11, are shown.

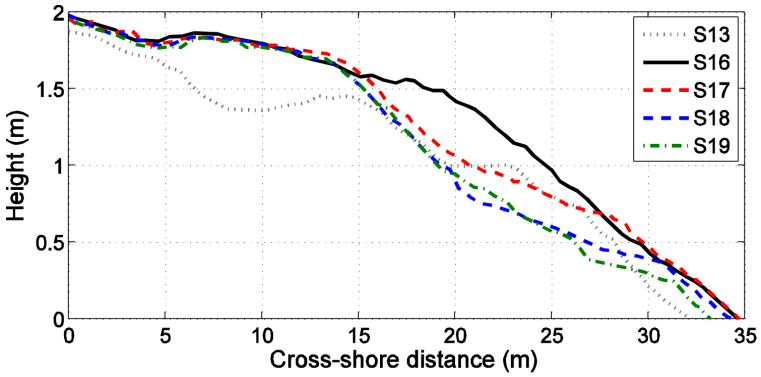

Figure 6: Pre-nourished upper profile and evolution since the artificial replenishment until the end of the study period in study area 1. Height = 0 indicates the MLWS level.

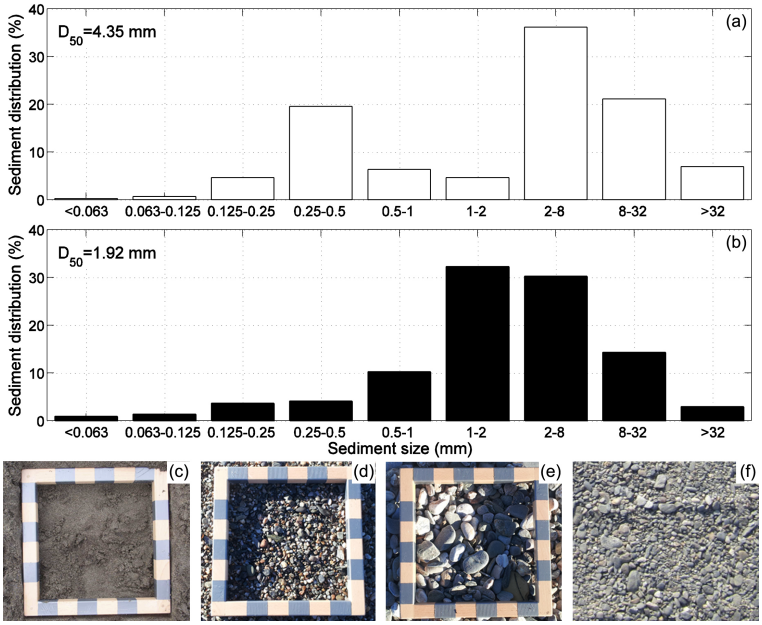

Figure 7: Grain size histograms of the set of samples in both study areas before the artificial replenishment (a) and of the sediments used for the artificial replenishment (b); sand (c), fine gravel (d) and coarse gravel (e) natural fractions; and sediments supplied in June 2014 (f). The D_{50} of the nourishment was lower than that of the natural sediment.

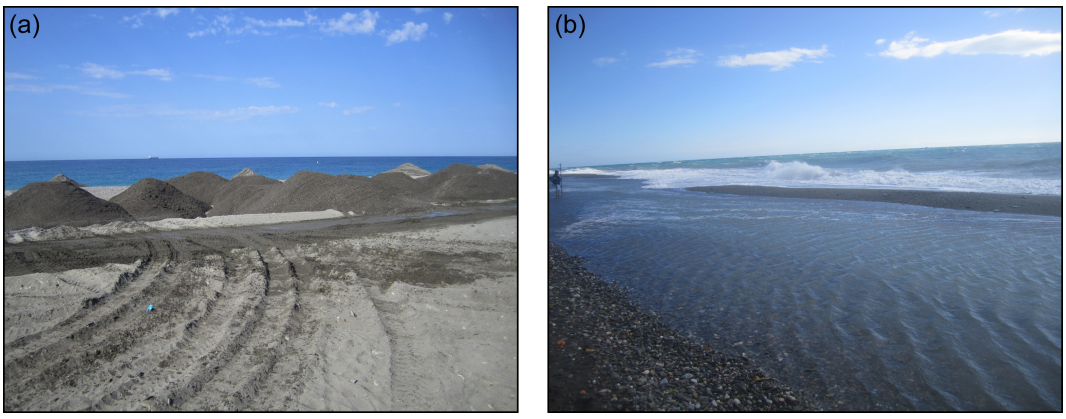

Figure 8: (a) Artificial replenishment done in June 2014, consisting of an input of sediment with uniform distribution. (b) Upper profile after the storm 1: Gravels on the storm berm and the surface layer of sand on the bar feature are observed.

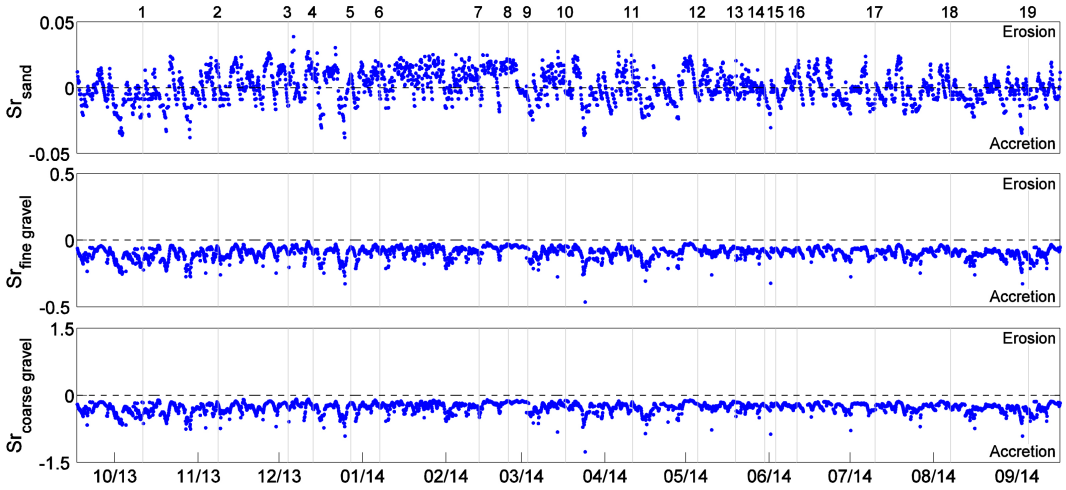

Figure 9: Difference between the terms of erosion and accretion in the Equation 1 (Sunamura and Takeda, 1984) in study area 1. The three prevailing sediment sizes were considered: sand (upper panel), fine gravel (middle panel) and coarse gravel (lower panel). The vertical lines (grey) indicate the date of the field surveys.

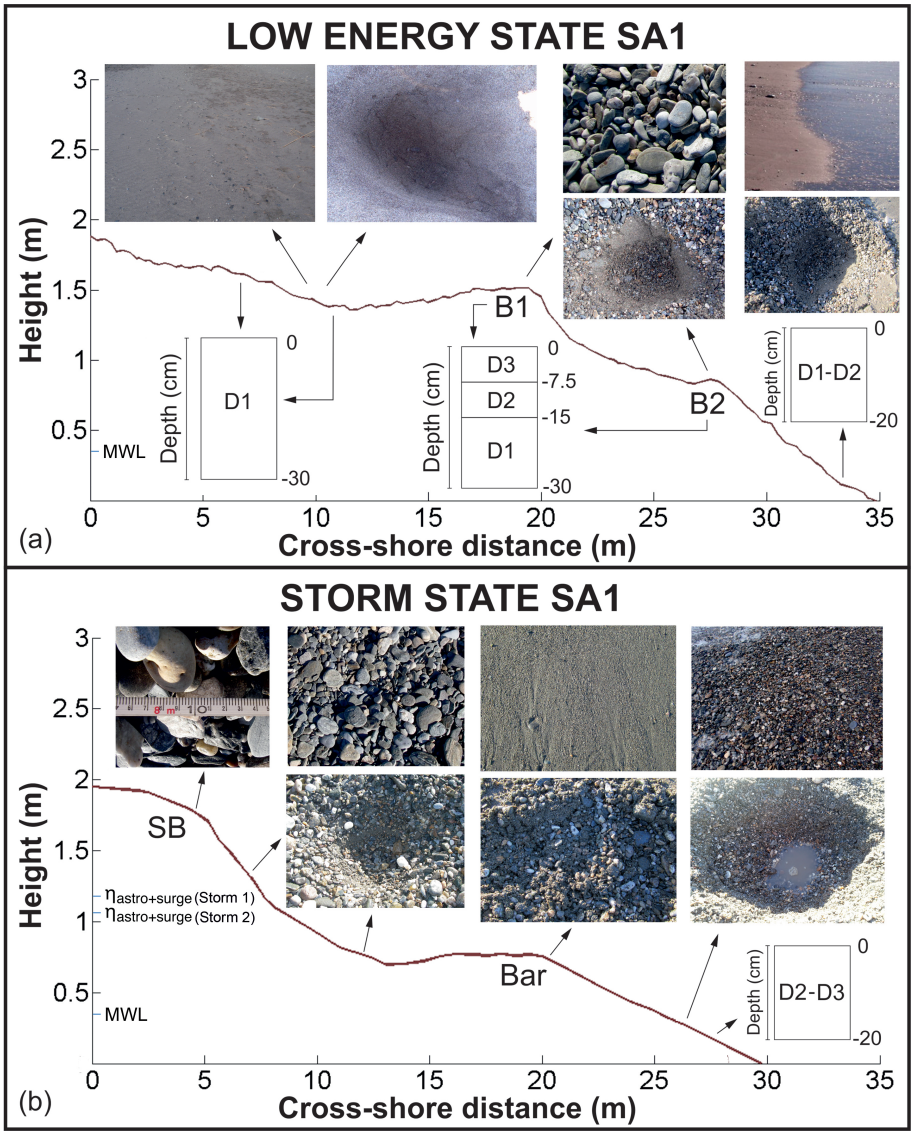

Figure 10: (a) Low energy state in study area 1: morphology (including the berms B1 and B2), sedimentology and photographs. (b) State after storms in study area 1: morphology (including the storm berm -SB- and the bar feature), sedimentology and photographs. Height = 0 indicates the MLWS level.

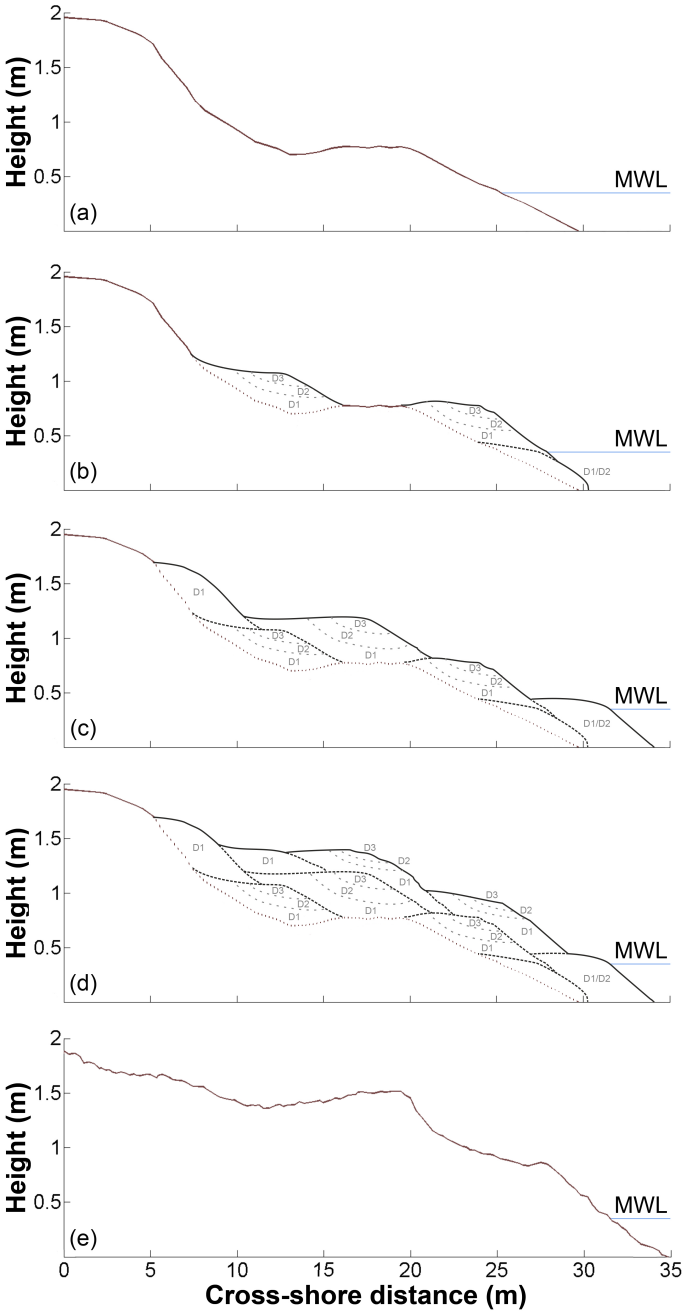

Figure 11: Conceptual model describing the beach's accretionary response in study area 1. From top to bottom: storm (S), transitional-storm (T-S), transitional (T), transitional-low energy (T-L) and low energy (L) states. The number of berms depends on the state of the beach profile.

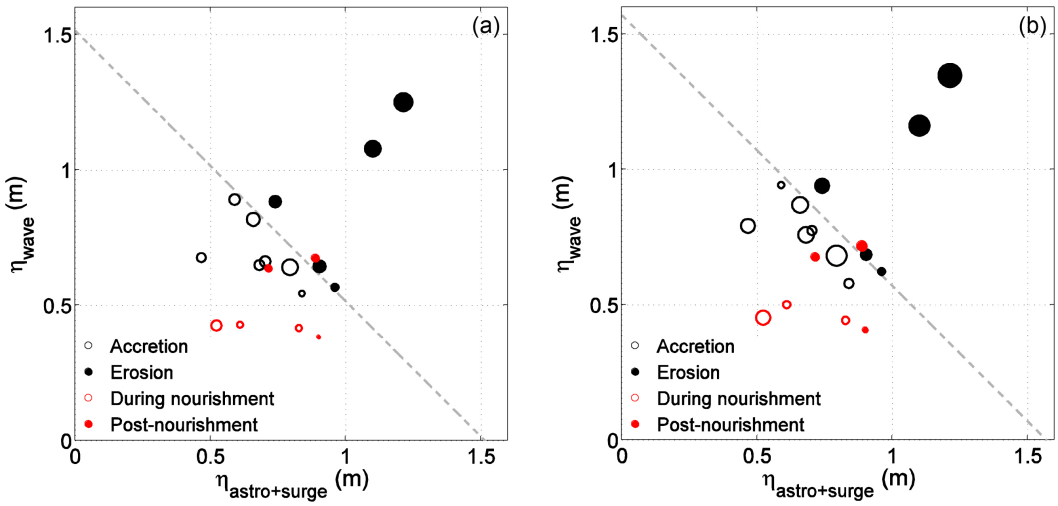

Figure 12: Relationship between the wave run-up and the water-level elevation in study areas 1 (a) and 2 (b). Black circles indicate accretion (unfilled) and erosion (filled) before the replenishment, whereas red circles indicate the artificial accretion (unfilled) and erosion (filled) afterwards. The size of the circles is proportional to the sediment volume change and the dashed grey line represents a total run-up of 1.52 m (a) and 1.58 (b).